JOURNAL OF MATERIALS SCIENCE 29 (1994) 4404–4414

AEM investigation of ceramic/Incoloy 909 diffusional reactions after joining by HIP

R. LARKER, L.-Y. WEI, B. LOBERG
Division of Engineering Materials, Luleå University of Technology, S-9751 87 Luleå, Sweden
M. OLSSON, S. JOHANSSON
Department of Materials Science, Uppsala University, S-751 21 Uppsala, Sweden

Diffusion bonding by hot isostatic pressing (HIP) was performed between Incoloy 909 and five different ceramics. Two of the ceramics were composites made from powder mixtures of Si_3N_4 and either 60 vol% TiN or 50 vol% TiB_2, while three were monolithic materials, namely Si_3N_4 with 2.5 wt% Y_2O_3 as a sintering additive, Si_3N_4 without additives, and Si_2N_2O without additives. A diffusion couple geometry was developed to facilitate the preparation of thin-foil specimens for examination by analytical electron microscopy (AEM). Diffusion bonding was performed by HIP at 927 °C (1200 K) and 200 MPa for 4 h. The formation of reaction layers was very limited, being less than 1 μm in total layer thickness. Two reaction products were found by AEM; a continuous, very thin, ($\leqslant$ 100 nm) layer of fine TiN crystals at the initial ceramic/metal interface, and larger grains extending about 100–500 nm into the superalloy and forming a semi-continuous layer of a G-phase silicide containing mainly nickel, silicon and niobium.

1. Introduction

Components intended to sustain a significant stress level at elevated temperatures (> 800 °C) can be manufactured from two classes of materials, either structural ceramics or metallic superalloys. Structural ceramics should, due to manufacturing limitations and costs, be applied only in parts where their properties can be utilized efficiently, mainly in components facing very high temperatures and/or aggressive environments at certain levels of mechanical or thermomechanical stress. Superalloys are preferred in all parts where their properties are sufficient. The utilization of silicon nitride (Si_3N_4) in hot applications such as heat engines is presently restricted by the lack of efficient joining methods to superalloys. Since an efficient use of these materials requires the joint to be positioned as far into the hot zone as possible, the joint must be able to withstand high temperatures (500–700 °C) during use and even higher temperatures during the formation of the joint. The possibilities for design with an efficient combination of these materials are strongly related the obtained durability of the joint.

Methods for ceramic/metal joints in structures used at elevated temperatures must deal with two major restrictions, namely the high residual stresses and excessive reaction layers that can occur in the bonded region during joining and use [1–6]. The strong covalent bonding in silicon nitride results in a lower coefficient of thermal expansion (CTE) than for most ceramics, while superalloys base their creep resistance on the FCC structure, causing a higher CTE than for ferritic steels. If silicon nitride and superalloys are rigidly joined, the thermally induced strains due to the large CTE mismatch result in extreme residual stresses that frequently cause fracture in the joint or some hundred microns into the ceramic [7–10].

2. Literature review

The main methods for joints between silicon nitride and metal alloys intended for use at elevated temperatures are diffusion bonding or active metal brazing. A recent literature review of these methods and the factors governing their durability [11] showed that most work has concerned methods to reduce the residual stresses by applying metallic interlayers in brazed or diffusion bonded joints. The frequently proposed solutions of changing the composition from the metal side through ductile metal interlayers such as nickel or copper [7, 12–17] and/or refractory metals such as tungsten or molybdenum [7, 9, 12, 14, 17–19] are difficult to protect against fatigue and oxidation, respectively [2]. The low-expansion characteristics of Invar and Kovar are restricted to relatively low temperatures (below 200 °C and 300 °C, respectively). In a recent study on Incoloy 909 [20], it was found that the benefit usually claimed for the use of this superalloy, a relatively low thermal expansion up to about 400 °C, is reduced by the considerably higher expansion in the range above 400 °C and up to the joining temperature.

Less work have been devoted to prevent the formation of excessive reaction layers with inferior mechanical and chemical properties at the interface. Furthermore, the necessity to retain the optimum

0022–2461

microstructure of the metal alloy after heat treatments experienced during joining has almost been ignored.

The two latter factors are very dependant of the temperature and hold time during joining. For applications with the highest requirements on joint durability, joining in the solid state by diffusion bonding is the prime choice. This is due to the possibilities of minimizing reaction zones and avoiding phases with low melting points and limited chemical stability. Most work on diffusion bonding with superalloys have, though, been conducted at very high temperatures (above 1000 °C) [7, 16,19], leading to the formation of thick reaction layers and probably excessive grain growth of the superalloy due to dissolution of grain-boundary precipitates. The formation of such reaction layers reduces the joint durability and thus the main advantage of diffusion bonding over brazing methods. The work on diffusion bonding between a dense HIPed β-sialon and pure nickel could be performed up to 1100 °C without the formation of thick reaction layers [12], possibly due to the lower reactivity when no nitride former is present at the interface to initiate the decomposition of Si_3N_4. The presence of the grain-boundary phase formed with additives of $MgO + Al_2O_3$ in sintered Si_3N_4 was found to increase the formation of reaction products [12, 14]. The influence on the formation of reaction products from the composition of the silicon nitride material used (such as grainboundary phase composition and impurity levels) has otherwise not attracted much attention, or occasionally not even been known [9].

The influences from the level and direction of applied pressure are often neglected. It could be useful to point out that a majority (four out of seven) of mechanisms used in the diffusion bonding model by Hill and Wallach [21] are directly or indirectly dependant on the level of the applied pressure.

Joint configurations other than the planar butt joint can be achieved by HIP. This method is presently considered to be an efficient sintering method for densifying powder bodies of metals or ceramics to fully dense components with close tolerances [22] or for defect healing of castings. The use of HIP for joining purposes has up to now mainly concerned diffusion bonding of different metal alloys, such as austenitic steel to ferritic steel, but the use of large HIP facilities could make diffusion bonding more accessible as a mass production process and increase the range of geometries that can be joined with diffusion bonding, according to Nicholas [3].

The high isostatic pressure (100–200 MPa) acting on the encapsulation of the joint pieces (evacuated before sealing and application of pressure) forces the metal at the joint interface to plasticize and accommodate to the surface of the ceramic. The yield strength of the metal alloy at joining temperature is usually lower than the applied HIP pressure, since, even for most superalloys, the major strengthening precipitates are dissolved at these temperatures. The major part of the void elimination can therefore be performed by yielding, mainly followed by power-law creep. This takes place without the shape distortion of the joint pieces that would occur if uniaxial pressure was applied up to this high level at the joining temperature, according to Suganuma [4]. The ability of superalloys to adapt to the very rough surface of a SiC/SiC continuous fibre composite during diffusion bonding by HIP was described by Larker *et al.* [23].

In contrast to other joining methods, such as active metal brazing or conventional diffusion bonding using vacuum hot pressing, the interfacial joining processes are taking place in a closed system inside the capsule. The pressurized encapsulation prevents both unwanted reactions with the furnace atmosphere and possible degradation by the formation of voids due to released gases, e.g. nitrogen during joining of silicon nitride.

These advantages for diffusion bonding by HIP permit reduction of bonding temperatures, resulting both in lower residual stresses and in a very thin interface, if chemical stability between the ceramic and the superalloy can be obtained. Moreover, the possibility of retaining the optimum microstructure in the metal alloy is increased with lower joining temperatures.

Concerning residual stresses, the main conclusion based on the review [11] was that in Si_3N_4/metal joints intended for high service temperatures (500–700 °C), the CTE mismatch could not be sufficiently reduced by modifying only the metal side of the joint. The composition in the ceramic part of the joint should therefore be graded to increase the thermal expansion behaviour from the low CTE value in monolithic silicon nitride up to a significantly higher value at the ceramic/metal interface. The supplementary ceramic phase in such graded particulate composites should fulfil the following requirements: (a) intermediate CTE; (b) sufficient stability against reactions with Si_3N_4 (during sintering); (c) useful properties of the particulate composite formed with Si_3N_4; (d) controlled reactivity against the superalloy (during joining and use). Titanium nitride (TiN) and titanium diboride (TiB_2) were found to possess suitable properties and were available in a variety of compositions, produced by ABB Cerama, Sweden, using glass-encapsulated HIP at 1600 °C. Dilatometric measurements showed that the steepest change in the mean CTE appears to take place in the interval 40–60 vol % of TiN or TiB_2, where both ceramic phases are continuous [24]. The value at 80 vol % TiN could reduce the CTE mismatch against Incoloy 909 to less than half from $\Delta\alpha = 8.8\ \mu m\ (m \times K)^{-1}$ to $\Delta\alpha = 3.5\ \mu m\ (m \times K)^{-1}$.

3. Materials and geometry for diffusion couples

3.1. Joined materials

The composite mainly treated in this paper was made from powder mixtures of Si_3N_4 and 60 vol % TiN, with an Y_2O_3 sintering additive level 4.0 wt % of the Si_3N_4 constituent.

Four other different ceramics were included in this study. One was a composite made from powder mixtures of Si_3N_4 and 50 vol % TiB_2, with an Y_2O_3 sintering additive level 0.3 wt % of the Si_3N_4 consti-

tuent. Three of the ceramics were monolithic materials, namely Si_3N_4 with 2.5 wt % Y_2O_3 as a sintering additive, Si_3N_4 without additives and Si_2N_2O without additives [25]. All five ceramics were sintered to theoretical density by glass-encapsulated HIP.

The superalloy used was Incoloy Alloy 909; (composition in wt %: 42.9 Fe, 37.4 Ni, 13.0 Co, 4.7 Nb, 1.5 Ti, 0.4 Si, $\leqslant$ 0.1 Al, 0.02 C). It was heat treated for optimum tensile properties by solution annealing at 980 °C/1 h/AC, followed by ageing at 720 °C/8 h/FC + 620 °C/8 h/AC [26].

3.2. Joining parameters

The joining temperature was chosen to be 1200 K (927 °C) considering results from thermodynamic calculations of possible reactions [5, 27, 28] and with the aim of retaining a useful microstructure in the superalloy after joining [20, 29]. The 200 MPa argon pressure level was the upper limit of the HIP equipment used, and the hold time was 4 h to permit the formation of relevant reaction products.

The reaction zones between diffusion bonded bulk samples of silicon nitride and Incoloy 909 have earlier [10] been shown to be very thin (1–2 μm), being below the spatial resolution limit for SEM/EDS. Recent work in TEM [12–15] has shown the possibilities of resolving the details of reaction products between silicon nitride and nickel. Due to the high yield strength of superalloys such as Incoloy 909 in comparison with pure nickel, the residual stresses can cause fracture in the joint or some hundred microns into the ceramic, where the stress level is highest [7, 10]. The stress level decreases with decreasing dimensions of the joint, but the handling during thinning and examination still involves a considerable risk for failure of the specimen.

It was therefore considered necessary to improve the joint configuration used in the preparation of thin-foil specimens for AEM studies.

3.3. Preparation methods

In a recent paper, Ishida *et al.* [30] discussed the difficulties associated with preparation of thin-foil specimens from ceramic–metal joints. A general difficulty is of course that the thinning process must be controlled so that both the reaction zone and the unreacted ceramic and metal on each side of the joint are thinned to electron transparency ($\leqslant$ 200 nm) without complete removal of any of these areas during the process. The positioning control is greatly enhanced by the use of dimple grinding and polishing with diamond slurries on one side of the specimen after planar grinding and polishing. The use of the dimple grinder can produce a specimen suitable for argon ion beam thinning where the centre has a thickness of only a few tens of microns, while the circumference giving the strength necessary for handling has a larger thickness (about 100 μm), determined in the planar grinding and polishing steps. This also decreases the time needed to reach sufficiently thin specimens, reducing the cost as well as the risk of contamination influencing the compositional measurements.

The thinning of the model combination Al_2O_3/Nb is facilitated by the almost equal thinning rates of these materials under the ion beam [30]. Unfortunately, this is not the case for joints between silicon nitride and metals [30]. For joints between two pieces of silicon nitride brazed with an Ag–Cu–Ti braze, the argon ion-beam thinning rates are so different that the two compound layers formed between the braze and the ceramic (mainly Ti_xSi_y and TiN) remained as relatively thick needles, while both Si_3N_4 and the Ag–Cu–Ti braze were thinned away. This selective thinning is so pronounced that the compound layer could resist the increased penetration depth of the 1 MeV beam in a high voltage electron microscope (HVEM). Off-centring of the ion beam from the joined interface was not enough to reduce the selective thinning. For a diffusion bonded joint between silicon nitride and nickel, the amorphous layer formed was instead thinned faster than the surroundings and appeared as a groove [30].

Diffusion couples with planar interfaces are not limited to the butt geometry when HIP is used, and the materials can instead be machined to a semicylindrical shape. The machining of the ceramic and metal materials to semicylinders before joining is more complicated, but this is more than equalized by the easier preparation of thin TEM specimens after joining.

The capsule tube adopts the shape of the joined semicylinders during HIP and can also form bonds to both of the joined materials. If the CTE value of the capsule material is higher than for the joined materials, the capsule would like to shrink more on cooling from the HIP temperature. This results in residual compression forces on the semicylinders, which is beneficial for the integrity of the joint when the joined couple is machined to prepare thin-foil specimens. For the joint between Si_3N_4 and Incoloy 909, capsules of either copper, mild steel or austenitic stainless steel would give this result. Stainless steel was chosen due to its combination of beneficial properties, such as a high CTE value, a rather high yield strength at room temperature, a non-magnetic behaviour and the availability of thin walled tubes in suitable dimensions.

3.4. Geometry of diffusion couples

Diffusion couples, designed to facilitate the subsequent preparation of thin-foil specimens, were fabricated according to the following route.

1. Ultrasonic machining of the five ceramics and electro-discharge machining of Incoloy 909 to cylindric samples with 2.32 mm diameter and 4.0 mm length.

2. Grinding lengthwise to obtain semicylinders with a planar surface (4.0 × 2.32 mm) on each sample.

3. Polishing of the planar surfaces using slurries down to 1 μm diamonds.

4. Encapsulation of paired ceramic/metal semicylinders in a stainless steel tube with 3.0 mm outer diameter and 2.35 mm inner diameter. The five different

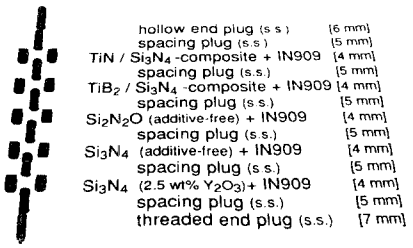

Figure 1 Configuration of ceramic and metal materials before encapsulation and diffusion bonding by HIP.

diffusion couples were separated axially by spacing plugs of stainless steel made with a waist-line in the middle of their 5 mm length to facilitate the positioning of later slice cutting (see Fig. 1 for complete configuration).

5. Diffusion bonding by HIP at 927 °C (1200 K) and 200 MPa for 4 h.

3.5. Preparation of thin-foil specimens

One of the diffusion couples, the one with Si_2N_2O, failed due to insufficient axial positioning during insertion of the five couples and six spacing plugs into the tube before sealing of the capsule. This could be observed after HIP but before cutting of thin slices, due to the different shape of the capsule at this position. The remaining four diffusion couples in the capsule were successfully bonded, and the preparation of thin-foil specimens was conducted in the following way.

1. Diamond wheel cutting of thin slices (400 μm) from the joined diffusion couples including a collar of the capsule. The number of slices from each couple could be maximized by observing the positions of the waistlines formed in the surface of the capsule at the middle of every spacing plug. Six or seven slices were obtained from each couple.

2. Planar grinding with SiC paper (1000 mesh followed by 4000 mesh) to about 70 μm thickness with the specimen mounted on a Gatan Disc Grinder.

3. Planar polishing in four steps using Struers DP-Spray on different DP-Cloths (6 μm diamonds on DP-Plan, 3 μm on DP-Plan, 1 μm on DP-Dur and 0.25 μm on DP-Nap) with the specimen held by a Gatan Disc Grinder.

4. Dimple grinding and polishing to about 7 μm final minimum thickness (measured using the narrow depth of focus at 1000× magnification in an optical microscope) using a Gatan Dimple Grinder with wheels of 15 mm diameter and with a 20 g load. Initially, grinding with 9 μm diamond paste was used down to about 25–30 μm thickness, followed by 6 μm paste down to about 20 μm thickness and 2.5 μm paste down to about 15 μm thickness. Polishing was then conducted with 1 μm and 0.25 μm paste down to the final minimum thickness.

5. Argon ion-beam thinning was finally used to obtain electron transparent areas of the joint interface using a Gatan Duomill at 5 kV and with a beam angle of 14° relative to the specimen plane. The specimen was rotated during thinning, and the effective thinning time was usually about 2 h.

During ion-beam thinning it was found that selective thinning was pronounced when the ion beam was parallel to the interface. Therefore, shields of stainless steel were attached on the holder of the rotating sample to avoid thinning when the angle of rotation was within ±45° of the direction parallel to the interface.

The reduced CTE mismatch in joints with the composites could be clearly observed by the markedly lower occurrence of cracks in slices with these ceramics compared to slices with the monolithic silicon nitride materials, especially the more brittle additive-free Si_3N_4. Cracking was not found closer than 200 μm to the ceramic/metal interfaces.

Due to the difference in polishing rate for the metal and the ceramic, the harder DP-Plan cloth was used down to 3 μm, followed by the DP-Dur instead of the softer DP-Mol cloth for the 1 μm diamonds.

The hardness of the ceramic part in the diffusion couple was found to markedly influence the dimpling speed with the coarser diamond pastes (9 μm and 6 μm). The composite with 50 vol % TiB_2 and the highest hardness ($H_{V0.5}$ = 20 GPa) was observed to require considerably longer dimpling time than the softest ceramic, the 60 vol % TiN composite ($H_{V0.5}$ = 15 GPa), while the two couples with monolithic Si_3N_4 were intermediate in both hardness and dimpling time.

The centre of the dimple grinding was initially positioned about 250 μm, into the ceramic. This was based on the presumption that Incoloy 909 would be less resistant to argon ion-beam thinning than the different ceramics. This was, however, only true for the diffusion couple with the 50 vol % TiB_2 composite. The pronounced topography observed in secondary electron images (SEI) showed that the Si_3N_4 phase was thinned much faster than the TiB_2 phase, and that it is possible that the TiB_2 grains to some extent shielded the Si_3N_4 grains from even faster thinning by the ion beam.

The monolithic Si_3N_4 materials were considerably less resistant than Incoloy 909 to the ion beam. The composite with 60 vol % TiN was also less resistant, although the TiN grains to some extent behaved in the same way as the TiB_2 grains. For optimum results it was therefore necessary to position the centre of the preceeding dimple grinding closer to the metal side. When the centre was positioned at the interface, the dimple drifted further into the softer metal, which was found beneficial after the subsequent ion-beam thinning. Therefore the centre of the dimple grinding was finally positioned about 250 μm into the metal for diffusion couples with the 60 vol % TiN composite or with the two monolithic Si_3N_4 materials.

This preparation route for thin-foil specimens was successful for the diffusion couples with the two composites. The ion-beam thinning of diffusion couples with the 50 vol % TiB_2 composite resulted in a hole on the metal side close to the interface, surrounded by electron-transparent areas, including the interface. It is beneficial for the contrast in transmission microscopy that the metal side is thinner than the ceramic side, because the higher specific density of the super-

alloy causes extinction of the electron beam for a smaller specimen thickness than is the case for the ceramic phases (in particular Si_3N_4). Since the Si_3N_4 grains were thinned more rapidly than both the superalloy and especially the TiB_2 grains, it was still difficult to find areas at the joint interface having both thin TiB_2 grains and adjacent remaining Si_3N_4 grains. The appearance of a thin foil specimen with the 50 vol % TiB_2 composite is shown in Fig. 2a.

Ion-beam thinning diffusion couples with the 60 vol % TiN composite initially resulted in a hole on the ceramic side of the interface, causing the metal side to be too thick for transmission of the electron beam. Changing the dimple grinding centre to be positioned at the interface resulted in a thin area on both sides of the interface. This limits, however, the interfacial areas it is possible to examine due to the rapid increase in thickness with increasing distance from the hole. Further change of dimple position into the metal resulted in a hole on the metal side close to the interface surrounded by electron-transparent areas, including the interface to the composite. Since the difference in thinning rate between grains of TiN and Si_3N_4 was much smaller than the large difference between TiB_2 and Si_3N_4, the ceramic grains were more evenly thinned in the 60 vol % TiN composite. The combination of thinner Si_3N_4 grains and their lower density (compared to TiN) still resulted in a large difference in image brightness between the grains in the ceramic composite. Two thin-foil specimens with the 60 vol % TiN composite, one dimpled with the initial dimple grinding position and the other with the final position, are shown in Fig. 2b and c, respectively.

The diffusion couples with the two monolithic Si_3N_4 materials proved to be more difficult to prepare, both due to fast thinning of the silicon nitride and to the considerably higher residual stresses in these couples from larger CTE mismatch [$\Delta\alpha = 8.8$ $(m \times K)^{-1}$] compared to the couples with the composites [$\Delta\alpha = 4.4$–5.9 μm $(m \times K)^{-1}$]. The large stresses often caused hemispherical cracking at a small distance from the interface, especially for the Si_3N_4 material HIPed without additives, having a lower fracture toughness. After dimpling at the initial position, the large difference in thinning rate caused the silicon nitride to be thinned away, while the metal side was still too thick to be transparent to the electron beam. Change of the dimpling position into the metal decreased the difference in thickness, but the silicon nitride grains were still usually much brighter than both the metal grains and the phases formed at the interface. The appearance of a thin-foil specimen with the monolithic silicon nitride (HIPed with 2.5 wt % yttria) (Y_2O_3) is shown in Fig. 2d.

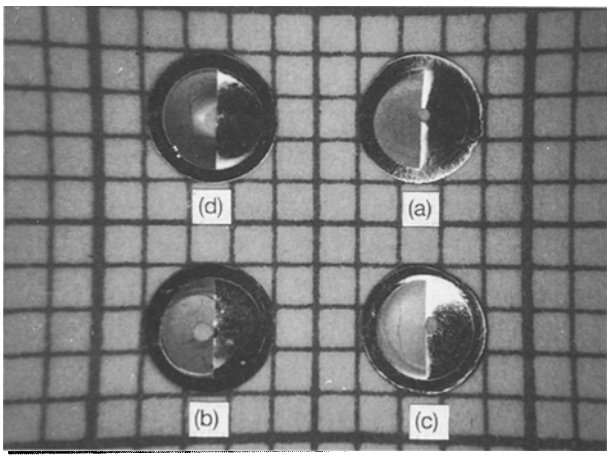

Figure 2 Thin-foil specimens after ion-beam thinning.

4. Analysis of diffusion reactions

4.1. Analytical electron microscopy

Most of the work was conducted with a Jeol JEM 2000-EX analytical electron microscope equipped with a Link AN 10000 system for EDS element analysis. The EDS detector was protected by a thin beryllium window; therefore the light elements nitrogen, boron, carbon and oxygen were omitted in the measurements while the remaining elements in the ceramics (silicon and titanium) and in the superalloy (iron, nickel, cobalt, niobium, titanium and silicon) were measured.

Two types of specimen holders were used; most work including the EDS elemental analysis was conducted with a graphite holder, while some structural investigations were conducted with a double-tilt holder. The specimens were consistently mounted with the interface of the joint perpendicular to the axial direction of the holder. Since the ceramic composites were electrically conductive, the specimens did not require carbon coating to avoid charging under the electron beam.

To obtain compositional profiles, quantitative microanalyses were conducted using the RTS-2/FLS programme. This programme compares the characteristic peaks of the acquired spectra with stored standard profiles for each pure element, and the energy scale is calibrated against a generated zero peak and the Cu K_α peak from a specimen of pure copper, measured during the same session at the microscope. Elemental concentrations were calculated using the thin foil approximation with corrections for absorption and normalized to 100 at % (nitrogen, boron, carbon and oxygen could not be detected). The points were normally positioned with 25 nm spacing along straight lines perpendicular to the interface, and since the electron beam of about 6 nm diameter while penetrating the thin foil (150–200 nm) broadens up to about 25–30 nm diameter, there is still only a slight overlap between consecutive points. The resulting spatial resolution is nearly two orders of magnitude higher than for quantitative point analyses with ZAF correction calculations, earlier conducted on bulk diffusion couples in SEM [10]. The acquiring time for each point was chosen to be 100 s.

4.2. Reaction phases found at the joint interfaces

The main impression from all of the joint interfaces examined is that the formation of reaction products is

very limited. The maximum total thickness of the reaction layers formed was below 1 μm. Two reaction phases could be readily observed in all specimens examined; the first phase was a continuous, about 100 nm thick layer (bright) consisting of numerous small crystals along the ceramic/metal interface, while the second was a semi-continuous layer (dark) of larger crystals formed with varying thickness in the superalloy. The characteristic appearance is shown in the diffusion bonded interface between the TiN/Si_3N_4 composite (left) and Incoloy 909 (right) in Fig. 3.

The relatively large grain to the left of the joint in Fig. 3 is a titanium nitride grain, while the adjacent silicon nitride grains above and below at the interface were almost absent, due to the higher thinning rates of these grains. Areas of interface with remaining silicon nitride adjacent to sufficiently thin titanium nitride grains could be found where a small Si_3N_4 grain was shielded by the more resistant TiN grains during ion beam thinning. An example of this is shown at lower magnification in Fig. 4a and a detail of the reaction zone adjacent to the Si_3N_4 grain is shown at higher magnification in Fig. 4b. Both reaction phases were more efficiently thinned adjacent to the Si_3N_4 grain, due to the increased exposure to the ion beam perpendicular to the interface when the thickness of the Si_3N_4 grain decreased.

The joint interfaces in diffusion couples with monolithic Si_3N_4 materials contained higher amounts of reaction products. This is shown in the diffusion bonded interface between Si_3N_4 (HIPed with 2.5 wt % yttria) (left) and Incoloy 909 (right) in Fig. 5. The formation of the crystals in the superalloy was larger

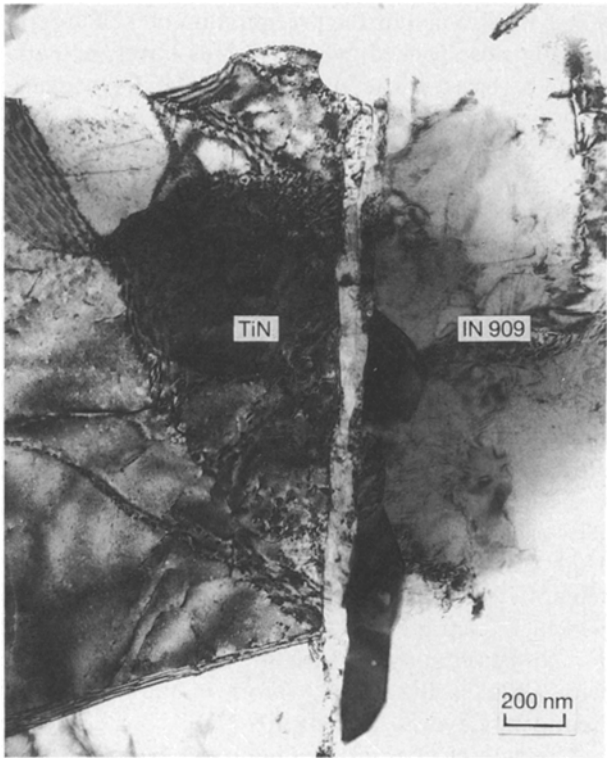

Figure 3 Reaction layers between the TiN/Si_3N_4 composite (left) and Incoloy 909 (right).

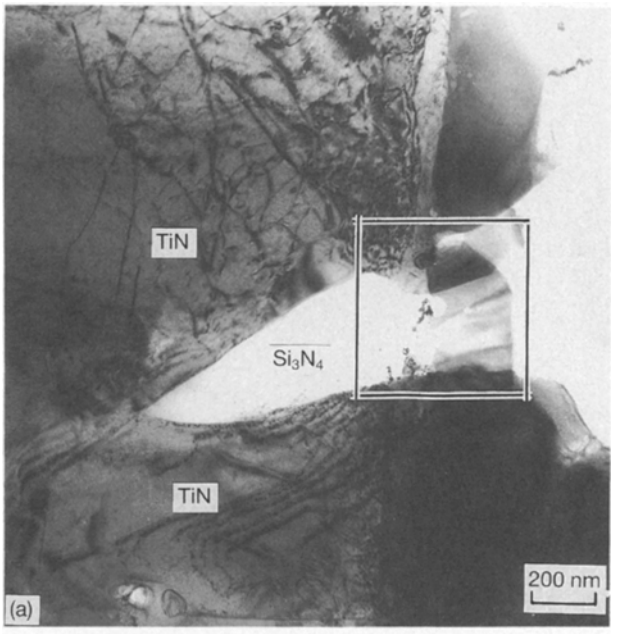

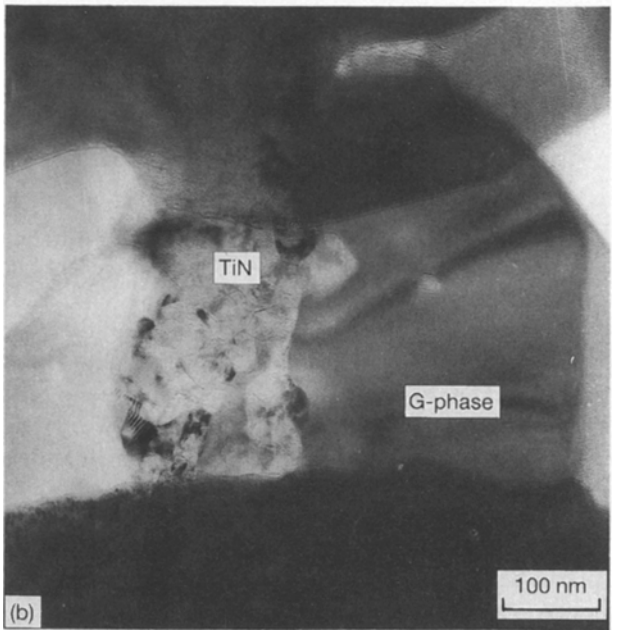

Figure 4 Phases formed at the interface with a Si_3N_4 grain (bright) in the TiN/Si_3N_4 composite: (a) overview; (b) detail of phases formed at the joint interface.

and almost continuous at interfaces with additive-free Si_3N_4.

4.2.1. Continuous reaction phase

The continuous layer between the ceramic grains and the grains of the semi-continuous reaction phase or the superalloy matrix contained clusters of very fine (< 50 nm) crystals. EDS point measurements resulted mainly in titanium peaks, and both selected area electron diffraction (SAED) and convergent beam electron diffraction (CBED) indicated that they were mainly TiN crystals. The crystals formed during joining are more than one order of magnitude smaller than the grains of the composite, but the EDS measurements could not distinguish between the crystals

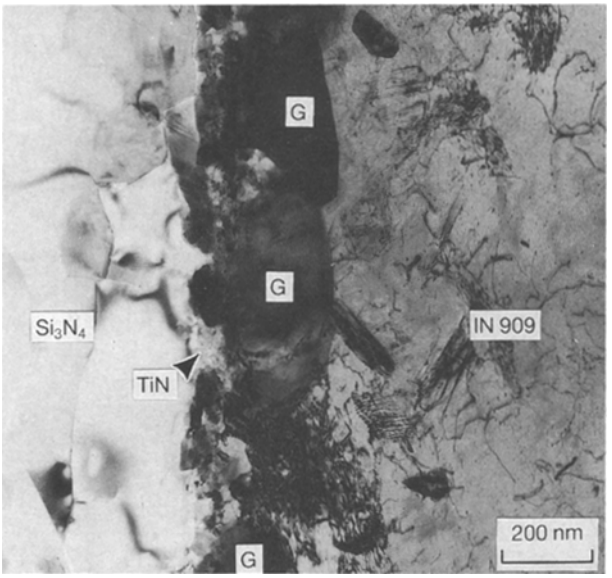

Figure 5 Phases formed between monolithic Si_3N_4 (HIPed with 2.5 wt% yttria) (left) and Incoloy 909 (right).

formed and the TiN or TiB_2 grains of the composites, since neither nitrogen nor boron could be detected.

4.2.2. Semi-continuous reaction phase

The thicker semi-continuous reaction phase consisted of seemingly defect-free grains elongated along the interface and was situated mainly in the superalloy close to the interface. Compositional profiles were determined along straight lines across these grains perpendicular to the interface by quantitative EDS point microanalysis with 25 nm spacing between consecutive points. A typical compositional profile for a wide grain of this phase is shown in Fig. 6.

This reaction phase was found to consist mainly of nickel, silicon and niobium. Enrichment of niobium and nickel is known to occur in all four major precipitates (γ', ε'', ε and Laves) in Incoloy 909 [29], but only ε and Laves have a higher content of niobium than titanium. Due to the higher content of silicon in Laves and to its globular shape (in contrast to the acicular ε), it was initially proposed [24] that the major reaction phase formed at the interface was a Laves phase.

That phase is known to form in grain boundaries at the high temperatures (800–1040 °C) routinely encountered during hot working and annealing [29, 31]. The shortest time for precipitation of Laves (< 0.1 h) is found at 870–930 °C in the time–temperature transformation (TTT) diagram [29, 31, 32]. Since the diffusion bonding was performed at 927 °C for 4 h, it was likely that Laves phase was formed. Such A_2B-type compounds are characterized by close-packed layers of slightly smaller A atoms (e.g. Fe, Co), separated by layers of slightly larger B atoms (e.g. Nb, Ti).

The formation of Laves phases is in general known to be stabilized by increased levels of silicon, niobium and titanium in Fe–Ni alloys [29, 33–36]. The grain-boundary Laves phase dominating in Incoloy 909 is of the hexagonal $MgZn_2$-type (C14) with the lattice parameters $a = 0.477$ nm and $c = 0.776$ nm [29]. Its formation is promoted by additions of silicon in Fe–Nb and Fe–Ti alloys [36] and by nickel in Co–Nb alloys [37], and it has an extensive solubility for silicon (up to 25–27 at %) in both Fe_2Nb [38] and Fe_2Ti [36] at 1100 °C. The silicon content measured in the five single grains of the major reaction phase could thus be on the solubility limit for these structures. One of the other two possible Laves structures, the cubic $MgCu_2$-type (C15), can be formed in Co–Nb alloys [38], but above about 5 at % Si, the structure changes to the hexagonal $MgZn_2$-type (C14), which is stable up to about 15 at % Si at 1100 °C. The extensions of the Laves phase regions along constant niobium lines in the Fe–Nb–Si and Co–Nb–Si systems indicate that silicon is substituting for iron and cobalt atoms, respectively [38].

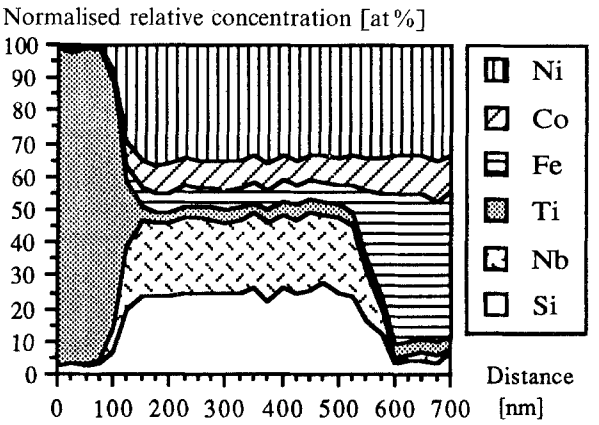

Figure 6 Compositional profile perpendicular to the interface from a relatively wide grain of the semi-continuous phase determined by quantitative EDS point microanalysis.

No Laves phases are, however, known to form in the Ni–Nb–Si or Ni–Ti–Si systems. While Fe-based alloys tend to favour the precipitation of TCP (topologically close-packed) phases such as Laves, σ, μ and χ, the Ni-based alloys instead favour GCP (geometrically close-packed) A_3B-type precipitates such as γ', η, γ'' or ε. This tendency is called the Laves–Wallbaum effect [34]. The size ratio between the atoms in the A_2B-type compounds would favour Laves phase formation between titanium or niobium as the slightly larger B element and nickel as the A element. The absence of such phases is attributed to an unfavourable electron/atom ratio [39].

Recent work by Savin [40] on the system Ni–Fe–Nb further showed that nickel-rich compositions prefer the orthorhombic δ-phase (Ni_3Nb) instead of Laves phases. The δ phase is formed during overageing of the ordered γ'' BCT (body-centered tetragonal) major strengthening phase in Inconel 718. High contents of silicon and niobium and low contents of aluminium promote this transformation, which is detrimental for the properties of such Fe–Ni–based alloys [33]. It is therefore not obvious why nickel is the main A atom in the A_2B grain-boundary Laves in Incoloy 909 [29].

These obscurities resulted in further examination of the semi-continuous reaction phase at the joint interfaces. Extensive SAED was conducted to characterize

its crystal structure. A low index SAED pattern was first obtained by tilting the specimen, as shown in Fig. 7a. By tilting around the two shortest reciprocal lattice vectors in this pattern, two series of SAED patterns were then obtained. The two projected reciprocal lattice planes which were perpendicular to the tilt axes, respectively, could be drawn up with the two systematic tilting series and so enabled determination of the reciprocal lattice unit cell and, as a consequence, the crystal lattice unit cell. The deduced Bravais lattice for this phase was FCC (face-centered cubic) with the lattice parameter $a = 1.13$ nm. The two low index patterns shown in Fig. 7a and b could therefore be indexed with the zone axes [1 0 0] and [1 1 0], respectively.

A further investigation using CBED (convergent beam electron diffraction) was conducted to confirm the FCC crystal structure of this reaction phase. The 4 m m symmetry deduced from the relative diffracted intensities in the HOLZ (high order Laue zone) rings further indicated that the major reaction phase had a FCC crystal lattice instead of a hexagonal lattice. The determined lattice parameter $a = 1.13$ nm was too large for a cubic Laves phase, and the silicon content in the major reaction phase was also too high for that structure, as earlier described.

The semi-continuous reaction phase must therefore be some other compound, that combines a large cubic lattice parameter with high contents of nickel, silicon and niobium. One such possibility is a ternary silicide called the G phase. It was first discovered by Beattie *et al.* in the Fe–Ni superalloy A-286, where a silicon content above 0.5 wt % caused precipitation of G phase in grain boundaries after solution treatment at 930 °C for 4 h followed by ageing at 650–815 °C for 1000 h; (the arbitrary name was assigned owing to its prominent appearance at grain boundaries) [35]. The presence of G phase in grain boundaries retarded grain growth, similar to the effect of Laves in Incoloy 909 [29].

Later work by Beattie *et al.* showed that G phase precipitated in nickel-rich and cobalt-rich complex austenitic alloys after solution treatment at 1205 °C for 8 h followed by ageing at 815 °C for 1000 h, on condition that the contents of Si and Ti were simultaneously high (about 1 wt % and 1.7 wt %, respectively) [34]. The G phase compositions suggested by Beattie *et al.* were $Ni_{13}Ti_8Si_6$ and $(Ni, Co)_{16}Ti_6Si_7$, respectively.

G phase silicides have recently been found as a minor phase in Incoloy 909 after prolonged exposure (> 100 h) at 820–1040 °C. Its composition was $Ni_{16}Nb_6Si_7$ (isostructural with $M_{23}C_6$ (116F)) [29]. Cobalt and titanium could substitute for nickel and niobium, respectively, in its structure [31].

Under the presumption that iron can also to some extent substitute for nickel in G phase, the compositions determined for the grains of the major reaction phase was found to fit well with both of the suggested compositions $Ni_{13}Ti_8Si_6$ and $Ni_{16}Nb_6Si_7$.

The lattice parameters for the cubic G phase silicides formed with titanium [$Ni_{13}Ti_8Si_6$ and $(Ni, Co)_{16}Ti_6Si_7$], characterized by Beattie *et al.*, were $a = 1.1198$ nm and $a = 1.1191$ nm, respectively, as determined by X-ray diffraction of extracted precipitates. An extensive determination of the lattice parameters for cubic G phases was conducted by Spiegel *et al.* [41]. According to the crystal structure, the $Ni_{16}Ti_6Si_7$ was considered to be the ideal composition. With Ni the lattice parameters of the G phase

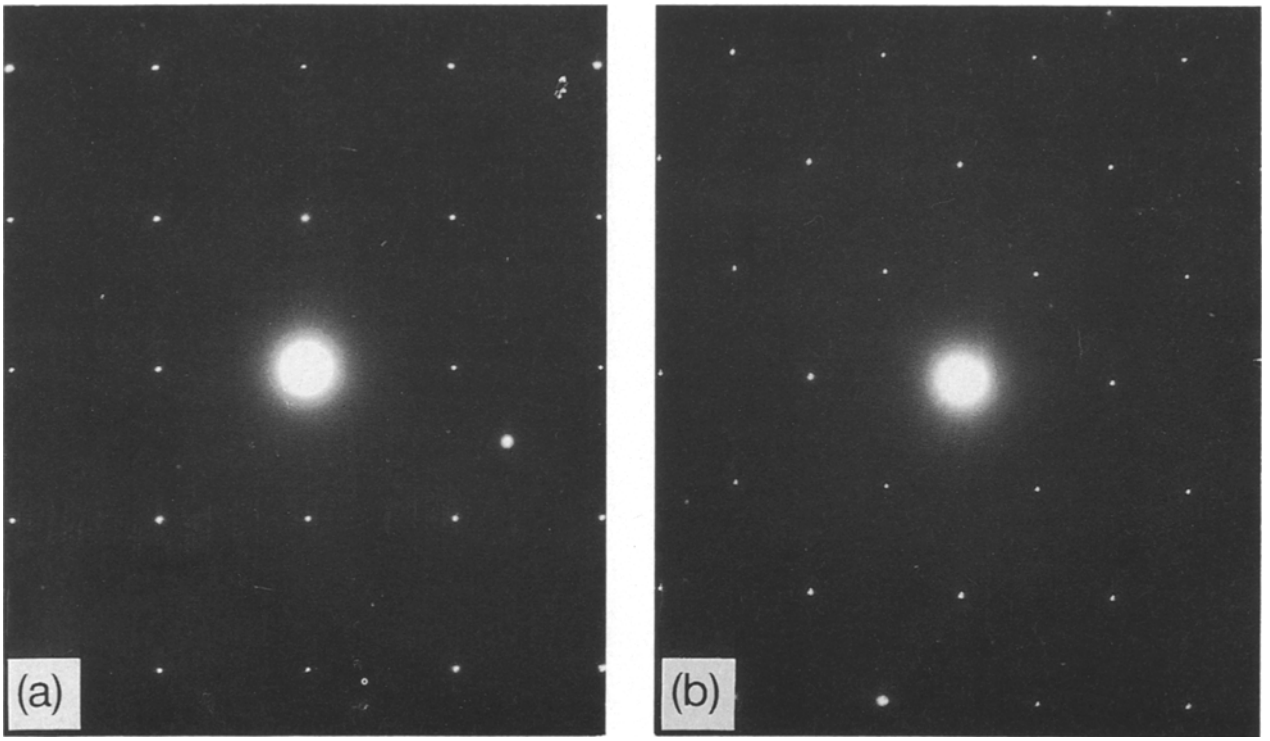

Figure 7 SAED patterns of the major semi-continuous reaction phase: (a) zone axis [1 0 0]; (b) zone axis [1 1 0].

were $a = 1.1187$ nm with Ti and $a = 1.1249$ nm with Nb, while for Co the lattice parameters were $a = 1.1201$ nm and $a = 1.1235$ nm, respectively.

The combination of nickel and titanium was the most effective in forming G phase, while iron was not found to form G phase with any transition element [41]. The lattice parameter for the cubic G phase silicide formed with niobium in Incoloy 909 ($Ni_{16}Nb_6Si_7$) was, by X-ray diffraction, determined to be $a = 1.125$ nm [29]. These values are in good agreement with the lattice parameter $a = 1.13$ nm for the major reaction phase formed at the joint interface, as determined by electron diffraction.

A third possible compound to form with the elements present at the joint interface and having a cubic structure with a large lattice parameter is Fe_2Nb_3. It has the lattice parameter $a = 1.1261$ nm [42], and it is isostructural with Ti_2Ni ($a = 1.1319$ nm [43]. The composition range of Fe_2Nb_3 is, however, restricted to 56–64 at % Nb and the maximum silicon solubility is about 6 at % at 1000 °C [42].

Since the semi-continuous reaction phase examined at the joint interfaces was single grains, and not agglomerates of different silicides, it was most probably a G phase silicide with some substitution of cobalt and iron for nickel and titanium for niobium. The main reason for its formation (instead of Laves phase) was probably the good supply of silicon at the joint interface, compared with the limited supply of silicon in the superalloy itself (1.2 at % Si in Incoloy 909). The source of niobium and titanium was mainly intragranular precipitates such as γ', ε'' and ε formed during ageing heat treatments (see Fig. 4). At the joining temperature, these precipitates (in particular γ') were more or less dissolved, facilitating diffusion of niobium and titanium towards the metal/ceramic interface. Some niobium might also come from the Laves precipitates already present in grain boundaries in the superalloy, intersected by the interface with the ceramics.

G phase was already formed at the joint interfaces after 4 h at 927 °C, which is considerably quicker than for precipitation in Si-containing alloys (> 100 h) described in the literature [29, 34, 35]. The main reason for this was probably the shorter diffusion path for silicon to the interface, compared with the diffusion to grain boundaries in alloys containing about 1 at % Si.

The formation of G phase was continuous along the interface with the composite containing TiB_2 but only semi-continuous for the composite containing TiN. This difference is probably due to the occurrence of free silicon in the former composite from a partial decomposition of TiB_2 and Si_3N_4 within the HIP capsule during densification, forming Si, BN and TiN together with the initial constituents. The formation of G phase with the monolithic Si_3N materials was larger than for the composite with TiN, probably due to the higher amount of silicon nitride present at the interface to react with nitride formers and silicide formers from the superalloy.

Occasionally, a third kind of reaction phase was found on the ceramic side in the specimens with the 50 vol % TiB_2 composite. Clusters of small grains, rich in silicon, nickel, iron and cobalt, were found in former Si_3N_4 areas. These clusters could be relatively large (up to 1 μm in size). It is likely that they contain silicides of nickel, iron and cobalt, promoted by the free silicon present.

4.3. Proposed reactions during joining

It is known from phase equilibria in ternary Me–Si–N systems that at temperatures up to 1000 °C, the potential silicide formers nickel, cobalt and iron are chemically inert to silicon nitride as long as nitrogen is not removed due to a low partial pressure of N_2 or by formation of nitrides with other metals [27, 44, 45]. Therefore the initial reactions must concern titanium and/or niobium. These metals are markedly reactive and form both nitrides and silicides with Si_3N_4 [5, 27, 44, 46].

For silicide formation between silicon nitride and these five metals, the largest negative free energy change ΔG is found for the formation of Nb_5Si_3, followed by Ti_5Si_3 and Ni_3Si, while at 1000 °C the free energy change is close to zero for Co_2Si and clearly positive for Fe_5Si_3 [5]. On the other hand, the free energy change (in kJ mol^{-1} of Si_3N_4) for Si_3N_4/metal reactions forming both nitrides and silicides show that ΔG for the formation of TiN + Ti_5Si_3 is very high, more than twice as high as for the formation of NbN + Nb_3Si [17].

This implies that titanium is the strongest nitride former present, and that the first reaction at the ceramic/metal interface is governed by the diffusion of titanium from the dissolved precipitates in the superalloy grains to the interface with silicon nitride, followed by decomposition of Si_3N_4 grains and formation of TiN crystals. The remaining silicon is then free to diffuse into the superalloy and together with the matrix and the constituents of the dissolved precipitates form the G phase silicide. This formation seems to be favoured instead of binary silicides with niobium, titanium and nickel.

5. Conclusions

Diffusion bonding of silicon nitride (Si_3N_4) ceramics to the low-expansion superalloy Incoloy 909 by HIP has shown to be efficient in several ways.

1. The metal surfaces have fully accommodated to the surfaces of the ceramics without macroscopic deformation of the diffusion couples, resulting in good adhesion and void-free joints.

2. The large residual stresses formed in the Si_3N_4–metal joints during cooling caused cracking in the ceramics about 200 μm from the joint interface, but the decreased CTE mismatch with the ceramic composites containing titanium nitride (TiN) or titanium diboride (TiB_2) considerably reduced cracking problems during preparation of thin-foil specimens for analytical electron microscopy (AEM).

3. Two reaction products were found by AEM after 4 h at 927 °C; a continuous, very thin (⩽ 100 nm) layer of fine TiN crystals at the initial ceramic/metal interface, and larger grains usually forming a semi-

continuous layer of a G phase silicide containing mainly nickel, silicon and niobium extending about 100–500 nm into the superalloy.

4. The proposed reaction is initiated by the diffusion of titanium from the dissolved precipitates in the superalloy grains to the interface with silicon nitride, followed by decomposition of Si_3N_4 grains and formation of TiN crystals. The remaining silicon is then free to diffuse into the superalloy and will, together with the matrix and the constituents of the dissolved precipitates, form the G phase silicide. This formation seems to be favoured instead of binary silicides with niobium, titanium and nickel.

5. The joining temperatures used (927 °C) is within the temperature range suitable for heat treatment of the superalloy. Excessive grain growth of formation of possibly embrittling phases in the superalloy have therefore been avoided. Joining could possibly be combined with annealing, later followed by ageing of the joined superalloy.

A possible way to assemble a joint resistant to fatigue and corrosion during thermal cycling up to 500–700 °C in oxidizing environments like hot air or those present in engines is suggested based on the experiences described in this paper.

1. The use of a functionally graded material (FGM) with increasing amounts of titanium nitride up to around 80 vol % TiN at the ceramic/metal interface might reduce the residual stresses to less than half of the stress level in Si_3N_4–Incoloy 909 joints.

2. Long-term stability might be provided due to the following three factors.

(a) The composition of the graded composite at the ceramic/metal interface (around 80 vol % TiN) entails that the silicon nitride grains present at the interface during joining are isolated. If these Si_3N_4 grains (of about 1 μm in size) are completely reacted to form TiN and G phase, further reactions will be inhibited due to the continuous TiN composite acting as a diffusion barrier.

(b) Most of the titanium and niobium is, after ageing, locked up in precipitates in the superalloy.

(c) The maximum temperature experienced by the joint in use is about 200 °C lower than the joining temperature.

3. Further reduction of residual stresses might be possible by adapting a cermet composition of TiN and a low-expansion metal alloy between the functionally graded ceramic and the metal alloy.

References

1. G. ELSSNER and G. PETZOW, *ISIJ Internat.* **30** (1990) 1011.
2. L. PEJRYD, in Proceedings of the 4th International Symposium on Ceramic Materials & Components for Engines, Gothenburg, Sweden, 1991, edited by R. Carlsson (Elsevier Applied Science 1992) p. 50.
3. M. G. NICHOLAS, in Proceedings of the International Institute of Welding Congress on Joining Research, 1990, edited by T. H. North (Chapman and Hall, 1991) p. 160.
4. K. SUGANUMA, *ISIJ Internat.* **30** (1990) 1046.
5. T. OKAMOTO, *ibid.* **30** (1990) 1033.
6. K. SUGANUMA, *Ann. Rev. Mater. Sci.* **18** (1988) 47.
7. T. YAMADA, H. SEKIGUCHI, H. OKAMOTO, S. AZUMA, A. KITAMURA and K. FUKAYA, *High Temp. Technol.* **5** (1987) 193.
8. K. SUGANUMA, T. OKAMOTO, M. KOIZUMI and M. SHIMADA, *J. Amer. Ceram. Soc.* **68** (1985) C-334.
9. M. L. SANTELLA, *Adv. Ceram. Mater.* **3** (1988) 457.
10. R. LARKER, B. LOBERG and T. JOHANSSON, in Proceedings of the 3rd International Symposium on Ceramic Materials & Components for Engines, Las Vegas, USA, edited by V. J. Tennery (American Ceramic Society, 1989) p. 503.
11. R. LARKER, Doctoral Thesis, Luleå University of Technology, Sweden (1992) ISSN 0348–8373.
12. T. ISHIKAWA, M. E. BRITO, Y. INOUE, Y. HIROTSU and A. MIYAMOTO, *ISIJ Internat.* **30** (1990) 1071.
13. M. E. BRITO, Doctoral Thesis, Nagaoka University of Technology, Japan (1989).
14. M. E. BRITO, H. YOKOYAMA, Y. HIROTSU and Y. MUTOH, *ISIJ Internat.* **29** (1989) 253.
15. K. SUGANUMA, K. NIIHARA and T. FUJITA, *J. Less-Common Metals* **158** (1990) 59.
16. A. FRISCH, W. A. KAYSSER, W. ZHANG and G. PETZOW, Proceedings of the 3rd International Conference on Hot Isostatic Pressing - HIP'91, Osaka, Japan, 1991, edited by M. Koizumi (Elsevier, 1992) p. 319.
17. Y. NAKAO, K. NISHIMOTO and K. SAIDA, *ISIJ Internat.* **30** (1991) 1142.
18. K. SUGANUMA, T. OKAMOTO, Y. MIYAMOTO, M. SHIMADA and M. KOIZUMI, *Mater. Sci. Technol.* **2** (1986) 1156.
19. A. FRISCH, W. A. KAYSSER, W. ZHANG, R. FELDMANN and G. PETZOW, in World Conference on Powder Metallurgy, Vol. 2, London, UK, 1990. (The Institute of Metals, 1990) p. 52.
20. R. LARKER, K. ANEVIK, S. KRISTIANSSON and B. LOBERG, *Mater. & Design* **13** (1992) 88.
21. A. HILL and E. R. WALLACH, *Acta Metall.* **37** (1989) 2425.
22. H. T. LARKER, in "Engineered materials handbook", Vol. 4, Ceramics and Glasses, edited by S. J. Schneider (ASM International, Materials park, Ohio, 1991) 194.
23. R. LARKER, A. NISSEN, L. PEJRYD and B. LOBERG, *Acta Metall. Mater.* **40** (1992) 3129.
24. R. LARKER, L. -Y. WEI, M. OLSSON and B. LOBERG, in Proceedings of the 4th International Symposium on Ceramic Materials & Components for Engines, Gothenburg, Sweden, 1991, edited by R. Carlsson (Elsevier Applied Science, 1992) p. 340.
25. R. LARKER, *J. Amer. Ceram. Soc.* **75** (1992) 62.
26. Incoloy alloys 907 and 909, Wiggin Alloys Ltd., Hereford, UK, Publication number 3775 (September 1982, revised July 1983).
27. J. C. SCHUSTER, F. WEITZER, J. BAUER and H. NOWOTNY, *Mater. Sci. Eng.* **A105/106** (1988) 210.
28 R. E. LOEHMAN, A. P. TOMSIA, J. A. PASK and S. M. JOHNSON, *J. Amer. Ceram. Soc.* **73** (1990) 552.
29. K. A. HECK, D. F. SMITH, J. S. SMITH, D. A. WELLS and M. A. HOLDERBY, in "Superalloys 1988", edited by S. Reichman, D. N. Duhl, G. Maurer, S. Antolovich and C. Lund (The Metallurgical Society, 1988) p. 151.
30. Y. ISHIDA, J. -Y. WANG, T. SUGA and S. -I. TANAKA, in Proceedings of the International Workshop on Metal-Ceramic Interfaces, Santa Barbara, CA, USA 1989, edited by M. Rühle, A. G. Evans, M. F. Ashby and J. P. Hirth (Acta-Scripta Metallurgica Proceedings Series 4, Pergamon Press, 1990).
31. K. A. HECK, in "Physical metallurgy of controlled expansion Invar-type alloys", edited by K. C. Russell and D. F. Smith (The Minerals, Metals & Materials Society, Warrendale, PA, USA, 1990) p. 273.
32. D. F. SMITH and J. S. SMITH, *ibid.*, p. 253.
33. E. E. BROWN and D. R. MUZYKA, in "Superalloys II", edited by C. T. Sims, N. S. Stoloff and W. C. Hagel (Wiley-Interscience, 1987) p. 165.
34. H. J. BEATTIE and W. C. HAGEL, *Trans. Metall. Soc. AIME* **233** (1965) 277.
35. H. J. BEATTIE and W. C. HAGEL, *J. Metals* (1957) 911.

36. A. M. BARDOS, D. I. BARDOS and P. A. BECK, *Trans. Metall. Soc. AIME* **227** (1963) 991.
37. B. J. PIEARCEY, R. JACKSON and B. B. ARGENT, *J. Inst. Metals* **91** (1963) 257.
38. B. N. SINGH and K. P. GUPTA, *Metall. Trans.* **3** (1972) 1427.
39. J. G. FALLER and L. P. SKOLNICK, *Trans. Metall. Soc. AIME* **227** (1963) 687.
40. V. V. SAVIN, *Phys. Met. Metall.* **68** (1989) 140.
41. F. X. SPIEGEL, D. BARDOS and P. A. BECK, *Trans. Metall. Soc. AIME* **227** (1963) 575.
42. H. J. GOLDSCHMIDT, *J. Iron Steel Inst.* **194** (1960) 169.
43. M. H. MÜLLER and H. W. KNOTT, *Trans. Metall. Soc. AIME* **227** (1963) 674.
44. J. C. SCHUSTER, in Proceedings of the International Conference on Joining of Ceramics, Glass and Metal, Bad Nauheim, Germany, edited by W. Kraft (DGM Informationsgesellschaft, Oberursel, Germany, 1989) p. 313.
45. F. WEITZER and J. C. SCHUSTER, *J. Solid State Chem.* **70** (1987) 178.
46. J. C. SCHUSTER and H. NOWOTNY, in Proceedings of the International Plansee Seminar 11, Vol. 1, edited by H. Bildstein and H. M. Ortner (Reutte, Austria, 1985) p. 899.

Received 30 April 1992
and accepted 24 February 1993